

Relative stability, electronic structure, and magnetism of MnN and (Ga,Mn)N alloys

J. A. Chan, Jefferson Z. Liu, Hannes Raebiger, Stephan Lany, and Alex Zunger

National Renewable Energy Laboratory, Golden, Colorado 80401, USA

(Received 16 October 2008; published 18 November 2008)

Pure MnN and (Ga,Mn)N alloys are investigated using the *ab initio* generalized gradient approximation +*U* (GGA+*U*) or the hybrid-exchange density-functional (B3LYP) methods. These methods are found to predict dramatically different electronic structure, magnetic behavior, and relative stabilities compared to previous density-functional theory (DFT) calculations. A unique structural anomaly of MnN, in which local-density calculations fail to predict the experimentally observed distorted rocksalt as the ground-state structure, is resolved under the GGA+*U* and B3LYP formalisms. The magnetic configurations of MnN are studied and the results suggest the magnetic state of zinc-blende MnN might be complex. Epitaxial calculations are used to show that the epitaxial zinc-blende MnN can be stabilized on an InGaN substrate. The structural stability of (Ga,Mn)N alloys was examined and a crossover from the zinc-blende-stable alloy to the rocksalt-stable alloy at an Mn concentration of $\sim 65\%$ was found. The tendency for zinc-blende (Ga,Mn)N alloys to phase separate is described by an asymmetric spinodal phase diagram calculated from a mixed-basis cluster expansion. This predicts that precipitates will consist of Mn concentrations of ~ 5 and $\sim 50\%$ at typical experimental growth temperatures. Thus, pure antiferromagnetic MnN, previously thought to suppress the Curie temperature, will not be formed. The Curie temperature for the 50% phase is calculated to be $T_C=354$ K, indicating the possibility of high-temperature ferromagnetism in zinc-blende (Ga,Mn)N alloys due to precipitates.

DOI: [10.1103/PhysRevB.78.184109](https://doi.org/10.1103/PhysRevB.78.184109)

PACS number(s): 73.61.Ey, 71.15.Mb, 75.50.Pp, 72.80.Ga

I. INTRODUCTION

Manganese mononitride (MnN) exhibits unique characteristics among d^4 transition-metal compounds such as CrX(VI) or MnX(V) both in terms of its structural chemistry and magnetic spin configuration. Its partial solubility in III-V semiconductors and ensuing ferromagnetism (FM) has led to a general interest both in pure MnN and in diluted forms such as (Ga,Mn)N alloys. However, despite the success of approximate forms of density-functional theory (DFT) in describing the electronic structure and magnetic properties of many Mn and Cr mononitrides and monochalcogenides [Table I (Refs. 1–22)], the local-density approximation (LDA) and the generalized gradient approximation (GGA) are found to break down in the case of MnN, which has led to confusing and conflicting descriptions in the literature. In this work, we address these problems and offer simple solutions.

The unique structural anomaly of MnN—the rocksalt (RS) vs zinc-blende (ZB) stability problem: Binary d^4 transition-metal chalcogenides and pnictides crystallize in the sixfold coordinated (CN6) NiAs or rocksalt type structures (Table I). Curiously, the LDA/GGA approximations to the density-functional theory predict the ground state of MnN to be a fourfold coordinated (CN4) ZB structure, whereas the observed sixfold coordinated distorted RS form is ~ 115 meV/cation higher in energy, as described in previous literature^{3–5} and the present calculations [Fig. 1(b)]. This anomaly is significant because fourfold coordinated magnetic semiconductors feature prominently in proposed spintronic applications,^{23,24} and because alloys of ZB MnN with zinc-blende III-V compounds, such as Mn-doped GaN, AlN, and InN, occupy a central role in such scenarios. ZB MnN has therefore been the subject of numerous calculations.^{3–5,25–33} Recently, it has been suggested that the

observed distorted rocksalt ground state^{1,2,34–36} was stabilized by the presence of 4% nitrogen vacancies.³ However, MnN rocksalt structure samples have been reported to have the ideal 1:1 Mn:N stoichiometry.^{34–36} In this work, we will show that the structural LDA/GGA anomaly in MnN is due to the Mn spin-up highest occupied molecular orbitals (HOMO) being too high in energy and the spin-down lowest unoccupied molecular orbitals (LUMO) being too low, reflecting the underlying failure of the self-interaction to cancel. The error can be rectified by shifting down the occupied Mn *d* orbitals, for example, by using an GGA+*U* approach or hybrid density functionals. Figure 1(a) shows the results obtained via GGA+*U*, where the sixfold coordinated distorted rocksalt MnN with ideal stoichiometry is correctly predicted to be the ground-state structure. The electronic structure is also metallic³⁶ in the observed antiferromagnetic configuration and the lattice parameters, $a=4.288$ Å and $c=4.228$ Å, agree very well with the experimental values [$a=4.256$ Å and $c=4.189$ Å (Refs. 1 and 34)].³⁷

The complex magnetic behavior of rocksalt and zinc-blende MnN: The GGA+*U* functional predicts the experimentally observed antiferromagnetic (AF1) configuration to be the lowest energy for the rocksalt structure, and a half-metallic ferrimagnetic configuration (FI) for zinc blende. A level diagram model used to explain the magnetic stability in zinc-blende (Ga,Mn)N alloys³⁸ predicts structures with high-spin electronic structures to have FM configurations, leading to the conclusion that this model cannot be extended to explain the complicated magnetic behavior of MnN. The total energies of the FM and the various AF configurations that have been investigated are slightly above that of FI, suggesting that the real configuration of ZB MnN at equilibrium volumes might in fact be complex.

Can ferromagnetic zinc-blende MnN be stabilized epitaxially? Ferromagnetic spin coupling between 3*d* atoms with partially occupied orbitals can be stabilized by increasing the

TABLE I. Lowest energy magnetic states (FM, AF, FI and AF NC) of Mn and Cr pnictide and chalcogenide binaries in their CN6 ground-state structures and metastable ZB. The Curie temperature, T_C , and Néel temperature, T_N , for the CN6 structures, and energy differences and lattice mismatches between bulk ZB and CN6, are shown.

Binary	Expt. ground state (CN6)	Expt. magnetic state [T_C/T_N (K)]	Does LDA/GGA agree with expt. gr. state?	Lowest ZB magnetic state	Bulk ΔE (ZB–CN6) (meV/cation)	Bulk $(\Delta V/V)^{1/3}$ (ZB–CN6) (%)	Does LDA/GGA predict ZB to be stabilized epitaxially?
d^4 MnN	RS (distorted)	AF (650–660) ^a	No ^{b–c}	FI/AF NC ^d	353 (GGA+ U) –115 (GGA) ^d –136 (GGA) ^e	7 (GGA+ U) 3(GGA) ^d	Yes, $a_s^* > 4.75$ Å, FI/AF NC (GGA+ U) ^d
MnP	MnP type	AF NC(47) ^f	Yes ^g	FM	1156 ^e	3 ^e	
MnAs	NiAs	FM (318)	Yes ^{g,j}	FM ^{g,j}	816 ^e , 820 ^g	3 ^e	No ^{g,h}
MnSb	NiAs	FM (587) ^f	Yes ^j	FM ^j	816 ^e	4 ^e	
d^4 CrS	NiAs	AF	Yes ^g	AF ^g	240 ^g	13 ^g	Yes, $a_s^* > 5.8$ Å, AF ^g
CrSe	NiAs	AF (320) ^k	No ^{g,i}	FM ^g	310 ^k , 230 ^g	9 ^g	Yes, $a_s^* > 6.2$ Å, FM ^g
CrTe	NiAs	FM (340) ^k	Yes ^g	FM ^g	360 ^k , 300 ^g	7 ^g	No ^{g,v}
d^5 MnO	RS (distorted)	AF (118) ^l	Yes ^{m,n}				
MnS	RS (distorted)	AF (75–150) ^m	Yes ^{m,n}	AF ^{m,p}	330 ^m	7 ^m	o
MnSe	RS (distorted)	AF	Yes ^p	AF ^p			r
MnTe	NiAs	AF	Yes ^{p,q}	AF ^p	210 ^q		s
d^3 CrAs	NiAs	AF	Yes ^g	FM ^g	840 ^g	6 ^g	No ^{g,f}
CrSb	NiAs	AF	Yes ^g	FM ^g	1080 ^g	3 ^g	No ^{g,u}

^aReferences 1 and 2.

^bReferences 3 and 4.

^cLDA/GGA gives ZB as the ground state instead of RS.

^dThis work.

^eReference 5.

^fReference 6.

^gReference 7.

^hZB MnAs (FM) can be grown (Refs. 8 and 9).

ⁱLDA predicts Ni-As FM instead of AF as the ground state.

^jReferences 10 and 11.

^kReference 12.

^lReference 13.

^mReference 14.

ⁿHartree-Fock calculations.

^oMnS (AF) naturally crystallizes in ZB (Ref. 15).

^pReference 16.

^qReference 17.

^rZB MnSe (AF) can be grown (Ref. 18).

^sZB MnTe (AF) can be grown (Ref. 19).

^tZB CrAs (AF) can be grown (Ref. 20).

^uZB CrSb (FM) can be grown (Ref. 21).

^vZB CrTe (FM) can be grown (Ref. 22).

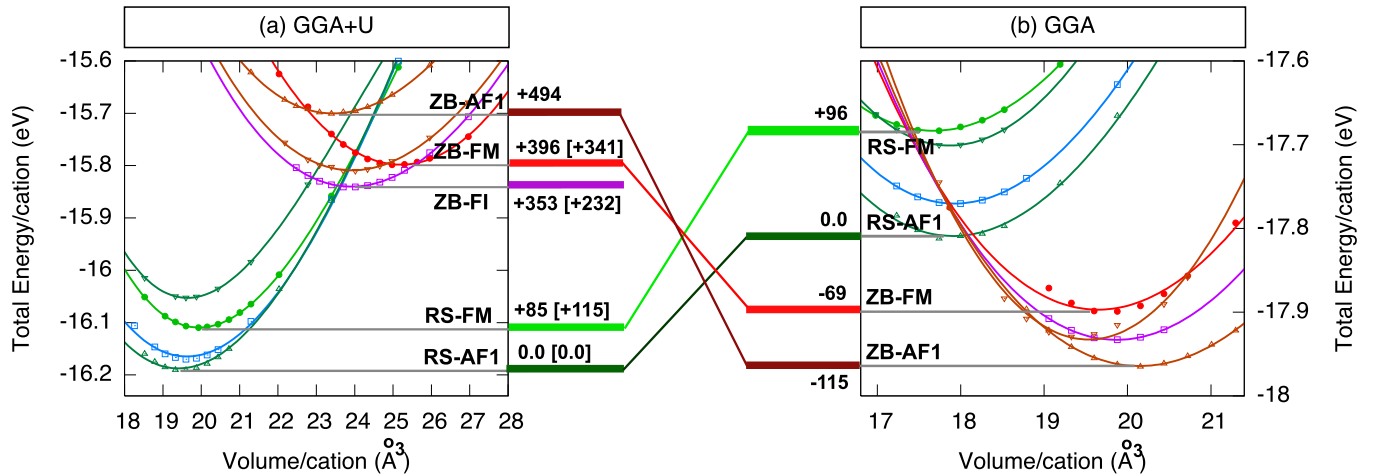


FIG. 1. (Color online) Total energies vs hydrostatic volume plots and relative energies for the RS (green/blue) and ZB (red/purple) phases as calculated by (a) GGA+ U and (b) GGA. B3LYP relative energies are given in square brackets. Magnetic states are FM (●), AF1–1 monolayer (001) (△), FI (□), and AF3–2 monolayers (001) (▽).

interatomic spacing.³⁹ This is because the ensuing narrowing of the bands could overcome the intra-atomic exchange interaction, which would otherwise lead to AF spin coupling. This trend is demonstrated in Table I by the transition from antiferromagnetism of the small lattice constant structure RS MnN to a mixed spin configuration in RS MnP and finally to a FM configuration in the larger lattice-constant structures RS MnAs and RS MnSb. Thus, an obvious way to design materials with a ferromagnetic spin configuration is to engineer volume expansion. Having established that the ZB structure of MnN, with a greater tendency for FM interactions compared to RS is higher in energy than the RS ground state [Fig. 1(a)], we next face the question of how to bring down the energy of the ZB structure. Volume expansion, in controlled experiments, cannot be achieved through simple hydrostatic means but by growing epitaxially on a substrate. In other words, in order to stabilize the fourfold coordinated ZB phase, one needs to explore the energy and spin configurations of ZB coherently confined in two dimensions to substrate lattice parameters. This may have an additional effect of changing the magnetic configuration. Previous theoretical calculations that investigated the stabilization of hydrostatically expanded fourfold coordinated magnetic compounds, in principle, should have included (biaxial) epitaxial geometries, not just (triaxial) hydrostatically expanded zinc-blende structures (Ref. 7 and references therein). Epitaxial calculations have been performed previously for a few 3d chalcogenides and pnictides (Table I), and the epitaxial ZB is found to only be stabilized with respect to the sixfold structures for CrS and CrSe. For ZB CrS, the magnetic configuration is AF, not FM. For ZB CrSe, a FM configuration may be expected but a substrate with sufficiently large lattice constant is not readily available. Here, we demonstrate epitaxial calculations of MnN both in the RS and the ZB phases, showing that on a substrate with lattice constant larger than 4.75 Å (10% larger than the equilibrium RS-MnN value of 4.3 Å) the epitaxial-ZB phase is thermodynamically more stable than the epitaxial RS.

Can zinc blende be stabilized over rocksalt by alloying with GaN? Another way to design volume expansion (i.e., increase the interatomic Mn-Mn separation) is to alloy MnN within a nonmagnetic host such as GaN. Indeed, homogeneous alloys such as (Ga,Mn)N and (Ga,Mn)As at dilute Mn concentrations are well known to exhibit ferromagnetism with (Ga,Mn)N predicted to achieve ferromagnetism above room temperature.⁴⁰ Given that, however, the ground state of Mn-rich (Ga,Mn)N (e.g., MnN itself) is sixfold coordinated rocksalt, it is important to establish at which composition range the fourfold structure is more stable than the sixfold structure. We compared the energies of the ZB and RS structures of the (Ga,Mn)N alloy, using supercells of “special quasirandom structures” (SQS), and found a crossover from the ZB-stable alloy to RS-stable alloy at a Mn concentration equal to or exceeding $x_{\text{Mn}} \sim 65\%$.

Phase separation in zinc-blende (Ga,Mn)N alloys may lead to high Curie temperature ferromagnetic precipitates: We next examine whether one can expect homogeneous phases or an inhomogeneous phase separation into Mn-rich and Ga-rich phases within the ZB-stable domain of the (Ga,Mn)N alloy. To this end, we will describe a cluster-

expansion (CE) calculation for the zinc-blende (Ga,Mn)N alloy based on over 40 total-energy GGA calculations. In this case, we apply a fixed moment approach that closely mimics the physics of the GGA+ U results of Fig. 1(a). The configurational total energies are mapped onto a generalized Ising-type expansion, and the magnitude and type of pair and many-body interactions are determined by this mapping. The ensuing interactions are then used to calculate the temperature-composition phase diagram. Previously published results, using the Korringa-Kohn-Rostoker (KKR) method within the coherent potential approximation (CPA), predicted a symmetric formation enthalpy vs Mn concentration curve, which implies a symmetric miscibility curve, thus, suggesting that the precipitates are essentially pure ZB MnN.⁴¹ Coupled with the LDA/GGA predictions that Mn-rich ZB alloys are AF,^{38,42,43} such results would lead to a prediction of a strong suppression of the Curie temperature, T_C , via the AF precipitates. In contrast, we find a strongly asymmetric phase diagram, suggesting that phase separation can occur into precipitates consisting of Mn concentrations of no more than $\sim 50\%$. Calculations on the high-concentration precipitates with $x_{\text{Mn}}=50\%$ show them to be ferromagnetic with a Curie temperature $T_C=354$ K in the mean-field approximation. FM that is due to precipitates may explain the observation of ferromagnetism in (Ga,Mn)N alloys.

II. DETAILS OF GGA, GGA+ U , AND B3LYP CALCULATIONS

The calculations were performed using *ab initio* DFT. The GGA and GGA+ U calculations utilized standard Perdew-Burke-Ernzerhof (PBE)-projector augmented wave (PAW) potentials, with a cutoff of 400 eV, and gamma-centered k -point sampling sufficient to converge the total energies to 0.1 meV/cation.⁴⁴ The fully relaxed geometry of each structure is optimized by relaxing the cell shape and internal coordinates with varying volume. For the GGA+ U calculations, $U=3.9$ and $J=1$ was applied to the Mn 3d orbitals. This value of U reproduces the correct thermochemical stability of MnO and Mn₂O₃,⁴⁵ and agrees with photoemission spectroscopy.⁴⁶ Similar values are used in previous calculations on (Ga,Mn)N.^{47,48}

The all-electron hybrid-exchange DFT calculations are performed using the B3LYP functional⁴⁹ (with 20% Hartree-Fock exchange), where the crystalline wave functions are expanded as a linear combination of atom-centered Gaussian orbitals (LCAO).⁵⁰ Structures are fully relaxed using the Broyden-Fletcher-Goldfarb-Shanno (BFGS) algorithm and triple valence basis sets are used: 86-411($d41$)G for Mn (Ref. 51) and 7-311G for N.⁵² The density of the reciprocal space sampling was enough to converge total energies to 0.1 meV/cation.

III. UNIQUE STRUCTURAL ANOMALY OF MnN—THE ROCKSALT VS ZINC-BLENDE STABILITY PROBLEM

Figure 1 shows the total energy vs hydrostatic volume of the different Mn phases, where the different spin configura-

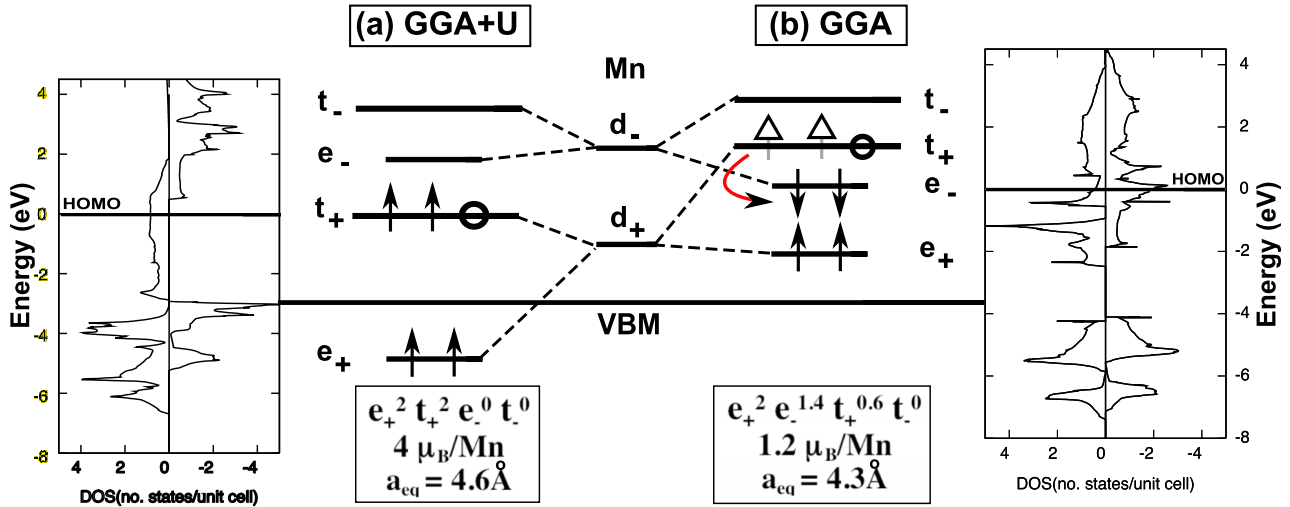


FIG. 2. (Color online) Total density of states of the ferromagnetic zinc-blende MnN in (a) the high-spin, half-metallic state (as predicted by GGA+ U) and (b) the low-spin, metallic state (predicted by GGA), with the HOMO and valence-band maximum (VBM) levels indicated. Corresponding energy levels resulting from Mn 3d (shown)-N p (not shown) interactions. Empty spin-up arrows indicate charge transfer from spin-up (\uparrow) t_+ to spin-down (\downarrow) e_- levels. Electronic configuration, magnetic moment (μ_B/Mn), and equilibrium lattice constant (a_{eq}) are shown.

rations of the rocksalt structure are represented by shades of green/blue and those for the zinc-blende structure are in shades of red. Considering only the structural energies, we see that, with the on-site Coulomb interaction [Fig. 1(a)], the distorted RS is correctly predicted as the ground state,^{1,34} with ZB being 353 meV/cation higher in energy. The opposite order is found when one uses GGA without U [Fig. 1(b)] in line with previous GGA calculations.^{3,5} The wurtzite phase (not shown), found to be 161(FM) – 244(AF1) meV/cation higher in energy than the respective phases of ZB in GGA, is comparable in energy in the GGA+ U description (13 – 20 meV/cation below ZB AF1 and FM energies, respectively).

**A. Model of electronic structure of MnN:
Effect of on-site Coulomb interaction**

The effect of U on the electronic density of states (DOS) is demonstrated in Fig. 2 using FM ZB MnN as an example. GGA describes the system as a low-spin, metallic state ($1.2\mu_B/\text{Mn}$, $e_+^2 e_-^{1.4} t_+^{0.6} t_-^0$) [Fig. 2(b)]. On the other hand, the GGA+ U description is one of a high-spin, half-metallic state ($4\mu_B/\text{Mn}$, $e_+^2 t_+^2 e_-^0 t_-^0$) [Fig. 2(a)]. The on-site Coulomb repulsion reduces the p - d coupling and increases the exchange splitting, which results in larger volume and half-metallic, integer magnetic moments for FM ZB and RS. This is in line with the shift of Mn d levels seen in previous LDA+ U calculations on dilute (Ga,Mn)N.^{47,48}

B. Validation of MnN results using the hybrid-exchange functional, B3LYP

In order to ascertain the reliability of the GGA+ U results, calculations with the hybrid-exchange functional, B3LYP, are also performed. B3LYP has been shown to give improved estimates for bandwidths and optical band gaps that are accurate as those obtained with sophisticated correlated calcu-

lations or perturbation methods.⁵³ The relative energies of various spin configurations as obtained by the hybrid functional [given in square brackets in Fig. 1(a)] agree very well with the GGA+ U results. The main features of the GGA+ U DOS are also reproduced by the B3LYP DOS (not shown), including the half-metallic FM states with $4\mu_B/\text{Mn}$ magnetic moment. The well-known LDA/GGA tendency for predicting spin-up Mn d levels too high and spin-down Mn d levels too low is therefore evident in this case.^{47,48} The dramatic and quantitative change in DOS on adding on-site Coulomb interaction is not expected in (Ga,Mn)As as the Mn d levels are located mainly within the valence band, not in the gap.

C. Relative stabilities of rocksalt and zinc-blende MnN

The change in relative stabilities of ZB and RS between the GGA and GGA+ U methods can be explained by how much each structure is stabilized in the GGA description. As Figure 1 shows, the energy gain in GGA relative to GGA+ U is 0.5 eV greater for ZB than for RS (while GGA and GGA+ U energies cannot be compared directly, the relative GGA-GGA+ U differences for the two structures can be compared). In GGA the charge transfer described in Fig. 2(b) between the occupied spin-up and unoccupied spin-down orbitals is much greater for ZB than RS. For example, for the FM state: for ZB the charge transferred is $1.4e$ [Fig. 2(b)] [from $4\mu_B/\text{Mn}$, $e_+^2 t_+^2 e_-^0 t_-^0$ (GGA+ U) to $1.2\mu_B/\text{Mn}$, $e_+^2 e_-^{1.4} t_+^{0.6} t_-^0$ (GGA)], and for RS the charge transferred is $1e$ [from $4\mu_B/\text{Mn}$, $t_+^3 e_+^1 t_-^0 e_-^0$ (GGA+ U) to $3.0\mu_B/\text{Mn}$, $t_+^3 t_-^{0.5} e_+^{0.5} e_-^0$ (GGA)]. Thus, in pure GGA, the stabilization with respect to the GGA+ U description is more for ZB than for RS.

**IV. THE COMPLEX MAGNETIC BEHAVIOR OF
ROCKSALT AND ZINC-BLENDE MnN**

A number of different magnetic configurations are calculated for RS and ZB structures: (i) FM, all spins parallel in

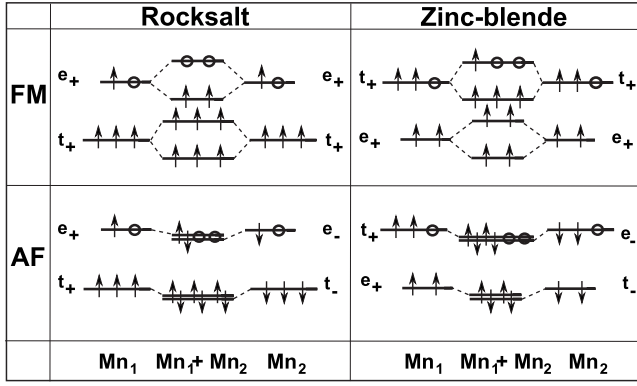


FIG. 3. Energy level diagrams of the magnetic interactions between two Mn ions (Mn_1 and Mn_2) in rocksalt and zinc-blende structures. The spin-up (\uparrow) and spin-down (\downarrow) electrons occupy the bonding or antibonding orbitals. Only the highest occupied orbitals are shown.

the ferromagnetic configuration, (ii) AF1, $(Mn\uparrow)_1/(Mn\downarrow)_1$ (001), i.e., monolayer alternation of spins in the (001) direction, (iii) FI, $(3e\uparrow, 1e\downarrow)$ in the 4 cation conventional cell, and (iv) AF3, $(Mn\uparrow)_2/(Mn\downarrow)_2$ (001), i.e., bilayer alternation spins in the (001) direction. Previous studies have focused mainly on the AF1 configuration as this was found to be the lowest magnetic configuration for both distorted RS (Refs. 4 and 54) and distorted ZB structures³¹ with the GGA approach [Fig. 1(b)]. We find that [Fig. 1(a)]: (i) Using GGA for ZB MnN, the AF1 state is predicted to be 62,²⁷ ~54,⁵ and 46 (this work) meV/cation lower in energy than FM. (ii) Using GGA+ U for ZB MnN, AF1 is 98 meV/cation higher in energy than FM, and FI is actually the lowest energy spin configuration found, being 43 meV/cation below FM. (iii) Using GGA for RS MnN, the lowest energy configuration is AF1, being 96 meV/cation below FM. (iv) Using GGA+ U for RS MnN gives AF1 as the magnetic ground state (85 meV/cation below FM), in agreement with experiment.^{1,34}

A level diagram previously used to explain the magnetic behavior of ZB (Ga,Mn)N alloys predicts low-spin electronic structures to have large $p-d$ coupling and small exchange splitting, and thus AF interactions are favored.³⁸ This seems to apply to the low-spin GGA results of MnN [Fig. 1(b)] as the antiferromagnetic configurations are lowest in energy. In contrast, high-spin configurations (Fig. 3) have smaller $p-d$ coupling (due to increase in cell volume) and larger exchange splitting. FM interactions should therefore be favored for both RS and ZB MnN (Fig. 3). Indeed, in Fig. 1(a), the high-spin GGA+ U results show that the AF configurations are not completely dominant over the FM interactions, and AF1 in fact becomes higher in energy than FM for ZB MnN. However, GGA+ U still gives the lowest energy configurations of RS and ZB to be antiferromagnetic and ferrimagnetic, respectively. This suggests that the mechanism in MnN is more complicated and the model needs to include effects such as orbital interaction strengths and bond directions.

The fact that the energies of AF3 and FM are just above that of FI suggests that the magnetic ground state of ZB MnN might be complex. MnP, a close relative of MnN, is known to exhibit noncollinear AF (AF NC) behavior at low

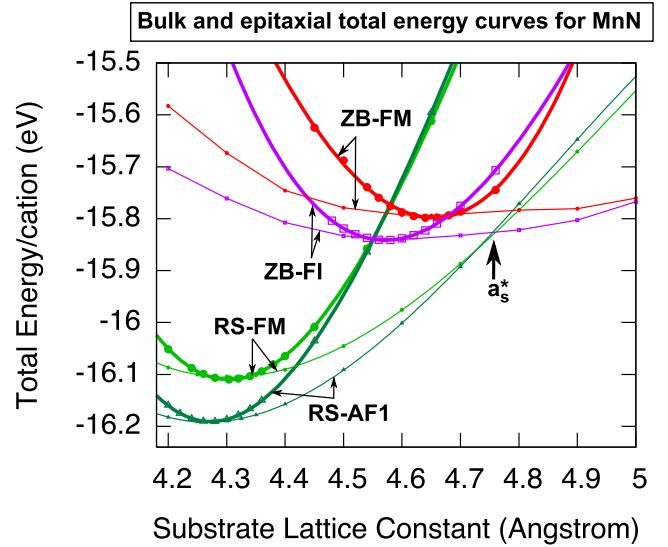


FIG. 4. (Color online) Total energies vs hydrostatic (thick lines) and epitaxial (thin lines) substrate lattice constants for different MnN phases. Magnetic states are FM (\bullet), AF1–1 monolayer (001) (Δ) and FI (\square). The a_s^* marks the substrate lattice constant where epitaxial zinc-blende becomes most stable.

temperatures below 47 K and is then FM up to 292 K.^{6,55} GGA calculations on vanadium arsenide suggest that dynamical electron correlations are important in describing the complex magnetic ground state.⁵⁶ Moreover recent calculations on MnAs indicate that spins deviate strongly from collinear ordering for low volumes whereas they align in a collinear ferromagnetic fashion for high volumes.⁵⁷ This suggests a complex magnetic arrangement for ZB MnN and similar compounds, and caution is required in describing the magnetic ground state of MnN and possibly also to related alloys.

V. CAN FERROMAGNETIC ZINC-BLENDE MnN BE STABILIZED EPITAXIALLY?

Figure 4 shows the total energy for hydrostatic (shown in thick lines) and epitaxial (thin lines) changes in volume for the RS and ZB structures. For the epitaxial calculations, the ZB or RS structures are made to coherently adhere to a substrate with lattice constant a_s (the x axis of the plot) whereas the remaining lattice direction (as well as cell internal degrees of freedom) are relaxed.⁷ The bulk and epitaxial curves coincide for a substrate with lattice constant that is equal to the natural bulk equilibrium value. When away from this lattice constant, the epitaxial curve is always lower in energy than the bulk curve because the epitaxial structure is relaxed in one dimension whereas the bulk is relaxed in all directions.⁷ The results for the FM and lowest energy configurations for each structure shows that: (i) Epi-ZB starts having lower energy than epi-RS for substrates with lattice constant a_s^* above 4.75 Å. This is 0.45 Å (or 10%) larger lattice constant than the equilibrium value of 4.3 Å for RS MnN. A suitable substrate might be an alloy of InGa_{0.45}N_{0.55}, with a ~43% In composition.⁵⁸ (ii) The lattice constant, a_s^* , at

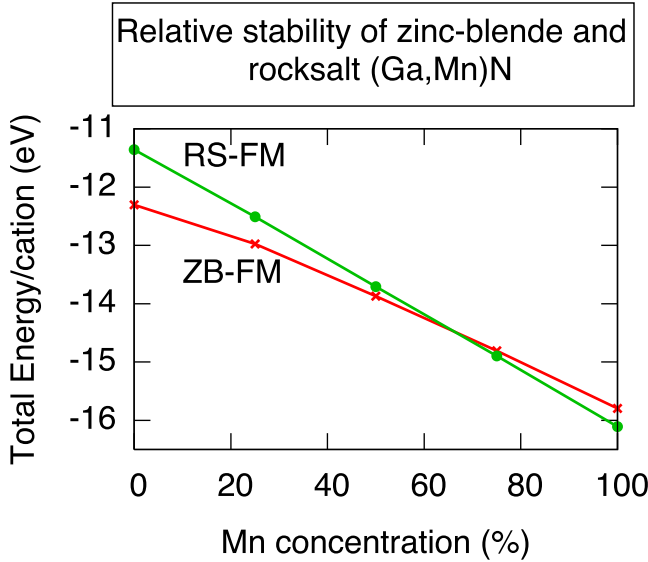


FIG. 5. (Color online) Total energies of RS and ZB special quasirandom structures of (Ga,Mn)N alloys at Mn concentrations of 25, 50, and 75%. The end points are given by the total energies of RS and ZB pure GaN and MnN.

which the crossover of epitaxial curves occurs is very different than the lattice constant at which the bulk RS and bulk ZB curves cross ($a=4.55 \text{ \AA}$). The latter crossing is, in fact, meaningless in terms of practical methods of achieving volume expansion. (iii) The stabilized epitaxial-ZB phase is the half-metallic FI spin configuration with $\sim 3.7\mu_B/\text{Mn}$. The half-metallic FM epitaxial ZB is 38 meV/cation higher in energy. Both AF and FM ZB phases are mechanically stable.

The findings show that ZB MnN can be grown in thermal equilibrium on a substrate such as InGaN. Many other materials, e.g., MnAs, MnS, etc. are predicted to be relatively unstable under epitaxial equilibrium conditions but are nevertheless observed in experiment (Table I). The calculations show how far from equilibrium the experimental conditions can be achieved and highlight potential cases for which special, nonequilibrium conditions are not required, therefore making them more viable materials for wider applications.

VI. CAN ZINC-BLENDE BE STABILIZED OVER ROCKSALT BY ALLOYING WITH GaN?

Since epitaxial stabilization of ZB MnN would appear to be possible but difficult, the natural progression for achieving volume expansion in order to obtain ferromagnetism is alloying. As the most stable forms of GaN are fourfold coordinated wurtzite and ZB (GaN has been observed in both structures), a crossing from RS, the ground state of MnN, to a fourfold coordinated lattice is expected on the mixing of MnN with GaN. We model the random ZB or RS alloy at varying concentrations using SQS fixed to cubic symmetry⁵⁹ (Fig. 5). The occupation of the lattice sites by Mn or Ga atoms is done in a controlled way so as to best mimic the atom-atom correlation functions of the corresponding infinite random arrangement. The SQS consist of 16 cations per unit cell, where the SQS structure at $x_{\text{Mn}}=50\%$ mimic the random

alloy up to the seventh nearest-neighbor (nn) pair, the seventh triplet, and the second quadruplets. The SQS at $x_{\text{Mn}}=25/75\%$ mimic the random alloy up to the third nn pair correlations and first triplet. The crossing point from RS to ZB, being the most stable, is found to be at an Mn concentration of $\sim 65\%$ (Fig. 5).

VII. PHASE-SEPARATION IN ZINC-BLENDE (Ga,Mn)N ALLOYS MAY LEAD TO HIGH CURIE TEMPERATURE FERROMAGNETIC PRECIPITATES

A. Details of Cluster Expansion calculations

To investigate the microscopic structure of (Ga,Mn)N alloys at the composition range where ZB alloys might be expected [Fig. 5], we have carried out a mixed-basis cluster expansion (MBCE). In a general cluster expansion, the formation energy, $\Delta E(\sigma)$, of a structure, $\sigma=s_0, s_1, \dots, s_N$ (i.e., a specific atomic occupation on each lattice), consisting of N numbers of atoms, can be expressed in terms of pair and many-body interactions:⁶⁰

$$\Delta E_{\text{CE}}(\sigma) = J_0 + \frac{1}{N} \left[\sum_i J_i s_i + \sum_{i,j} J_{ij} s_i s_j + \sum_{i,j,k} J_{ijk} s_i s_j s_k + \dots \right] + \sum_k \Delta E_{\text{CS}}(\hat{\mathbf{k}}, x) F(\mathbf{k}, \sigma) \quad (1)$$

where s_i is the spin variable ($s_i=-1$ or $s_i=1$ if site i is occupied by atom type A or B, respectively), the J_{ij}, J_{ijk}, \dots terms are the interaction energies of pair, three-body, etc. figures, and $F(\mathbf{k}, \sigma) = |S(\mathbf{k}, \sigma)|^2 e^{-|\mathbf{k}|^2} / 4x(1-x)$. The last term is used to describe the atomic size mismatch effects, in which the constituent strain energy term $\Delta E_{\text{CS}}(x, \hat{\mathbf{k}})$ is defined as the elastic energy cost to form lattice matching at the interface of two semi-infinite slabs AC and BC of orientation $\hat{\mathbf{k}}$. Since the lattice mismatch between GaN and MnN zinc-blende structures is small (less than 1%), the constituent strain energy is set to $\Delta E_{\text{CS}}(x, \hat{\mathbf{k}}) = 0$.

All the quantities which define the MBCE in Eq. (1) are determined by *ab initio* total-energy calculations. The interaction energies $\{J_{ij}, \dots\}$ are obtained by fitting $\Delta E_{\text{CE}}(\sigma)$ to a set of *ab initio* calculated formation energies $\{\Delta E_{\text{LDA}}(\sigma)\}$. The total-energy calculations are confined to the FM state and are obtained using the GGA functional with the total magnetic moment fixed to the integer moment of the half-metallic state. This ensures the correct electronic structure of the FM state [Fig. 2(a)] while simultaneously utilizing the GGA functional (that does not rely on the value of U). We consider this fixed moment GGA method to be more reliable for obtaining formation energies. The correct ordering of RS vs ZB for MnN is still obtained with ZB FM being 210 meV/cation higher in energy than RS FM. The directly calculated formation energies using this method are shown in Fig. 6.

A “leave-many-out” cross-validation (CV) score is adopted as a fitting quality parameter.⁶¹ The interactions are obtained by first eliminating several ordered structures from the fit and choosing the interactions that results in the best prediction error (i.e., the CV score) for the eliminated con-

Formula	x_{Mn} (%)	Nearest neighbor						
Ga₃₀Mn₂N₃₂	6.25	1st	2nd	3rd	4th	5th		
		30	47	45	40	47		
		Superslattice direction					Other structures	
Ga₇Mn₁N₈	12.5	(100)	(110)	(111)	(201)	(311)	2x2x2	
							68	
Ga₃Mn₁N₄	25	Z1	Y1	V1	DO₂₂	W1	L1₂	L1₃
		56	91	42	141	83	133	75
Ga₂Mn₁N₃	33.3	β2	γ2	α2	γ2	γ2		
		70	119	52	119	119		
Ga₁Mn₁N₂	50	L1₀	L1₀	L1₁	L1₀	L1₁		
		87	87	62	87	62		
Ga₂Mn₂N₄	50	Z2	Y2	V2	CH	W2		
		41	70	25	108	83		
Ga₁Mn₂N₃	66.7	β1	γ1	α1	γ1	γ1		
		45	79	30	79	79		
Ga₁Mn₃N₄	75	Z1	Y1	V1	DO₂₂	W1	L1₂	L1₃
		36	43	20	63	45	51	44

FIG. 6. Directly calculated formation enthalpies (meV/cation) for various ordered structures as input into the cluster expansion. Conventional names of the superslattice structures are also shown.

figurations. The process is repeated, including more GGA input structures at each step, until a desired accuracy is achieved. A good fit is obtained with 41 input structures, and with seven pair, five triplet, and three quadruplet figures. The final statistical prediction error (CV score) is 4.10 meV/cation. The resulting J interaction energies for the pair and many-body interactions are shown in Fig. 7.

The energy of random alloy is defined as the average of the formation energy over all possible atomic structures:

$$\Delta H_{\text{random}}(x) = \langle \Delta H(\sigma) \rangle = J_0 + J_1 \langle s_i \rangle + \sum_{ij} J_{ij} \langle s_i s_j \rangle + \sum_{ijk} J_{ijk} \langle s_i s_j s_k \rangle + \dots \quad (2)$$

In random alloys there are no correlations between different lattice sites and so the average of spin product is just simply equal to the product of spin average, i.e., $\langle s_i s_j \rangle = \langle s_i \rangle \langle s_j \rangle$. In addition, there is no distinction between different lattice sites. The averages of each individual spin variable (assigned to each lattice site) are equal and determined by the composition as $\langle s_i \rangle = \langle s_j \rangle = (2x - 1)$. The energy of the random alloy is therefore

$$\Delta H_{\text{random}}(x) = J_0 + J_1(2x - 1) + \sum_{ij} J_{ij}(2x - 1)^2 + \sum_{ijk} J_{ijk}(2x - 1)^3 + \dots \quad (3)$$

The free energy of random alloy is expressed as

$$G(x, T) = \Delta H_{\text{random}}(x) + k_B T [x \ln x + (1 - x) \ln(1 - x)]. \quad (4)$$

B. Prediction of an asymmetric x vs T spinodal phase diagram

Figure 8(a) shows the energies of the 2^{20} predicted configurations of ZB (Ga,Mn)N. The red line gives the energies

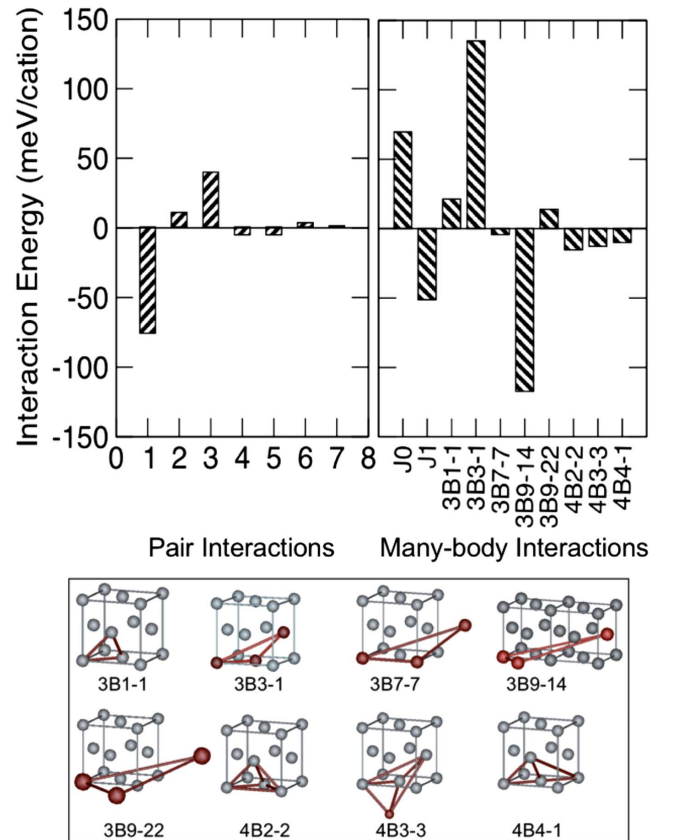


FIG. 7. (Color online) Energies of pair and many-body interactions for the converged cluster expansion of zinc-blende (Ga,Mn)N alloys. The geometries of the many-body figures are also shown.

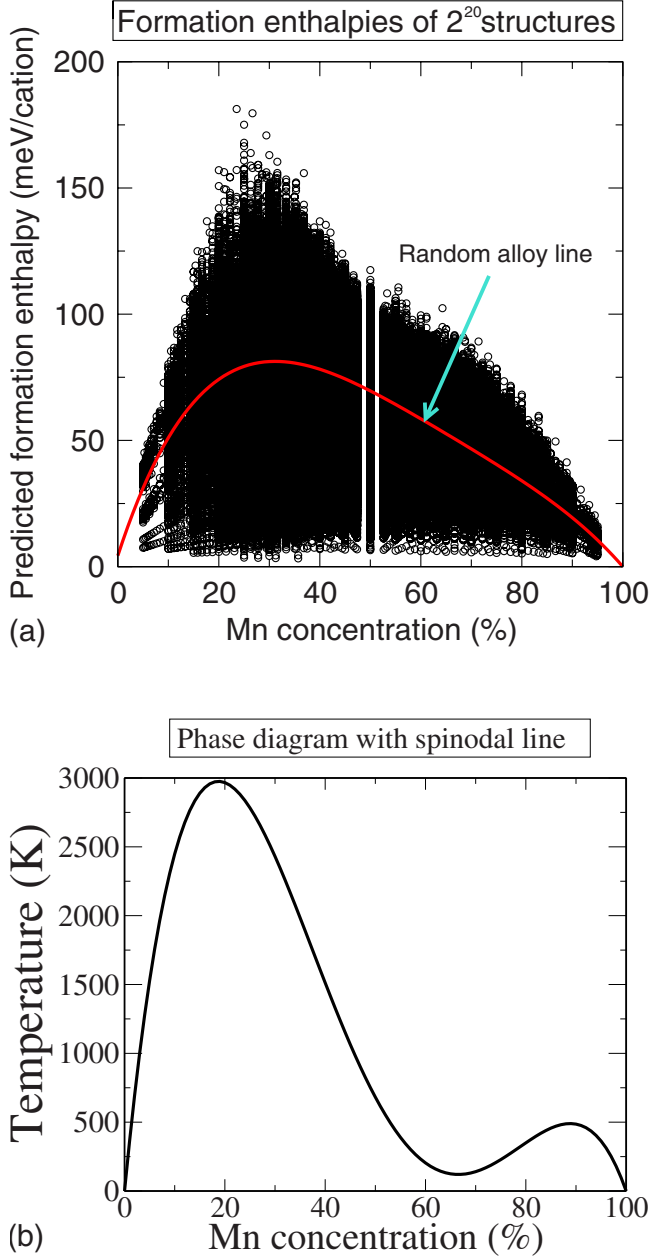


FIG. 8. (Color online) (a) Predicted formation enthalpies of 2^{20} structures with up to 20 cations/unit cell. The red line is the formation enthalpy of the random alloy. (b) The phase diagram showing the calculated spinodal line of zinc-blende (Ga,Mn)N alloys using the mean-field approximation.

of the random alloy. The spinodal decomposition line is then calculated by searching the composition where the second partial differential of free energy, $G(x, T)$, with respect to Mn composition, x_{Mn} , is equal to zero at a given temperature, T [Fig. 8(b)]. The miscibility-gap temperature, at the maximum of the spinodal line, is $T_{\text{MG}}=2975$ K at $x_{\text{Mn}}=19\%$. Below this temperature the alloy phase separates. The spinodal line has a negative curvature of $H-TS$ with respect to the Mn concentration, x_{Mn} . The ideal mixing entropy term, $-TS$, always has a positive curvature, whereas the formation energy, H , of the random solid solution leads to such a negative curvature and thus the instability. It is clear from Fig. 8(a)

that the curvature of the formation energy of the (Ga,Mn)N random alloy is smallest around $x_{\text{Mn}}=65\%$ (i.e., the curve is approximately linear). Between 200 and 500 K, at around $x_{\text{Mn}}=65\%$, the entropy contribution, $-TS$, can make the solid solution phase metastable (i.e., positive curvature of free energy), whereas outside this region, the formation energy term H dominates and the solid solution phase is unstable (i.e., negative curvature of free energy). This yields an unusual inverse-W shaped spinodal line.

We see in Fig. 8(a) that unlike the results obtained in previous literature (Fig. 1 in Ref. 41) formation energies of the random alloy vs Mn concentration are asymmetric, and thus the corresponding spinodal line is strongly asymmetric about $x_{\text{Mn}}=50\%$ [Fig. 8(a)]. At typical growth temperatures (500–1000 K), the (Ga,Mn)N alloy would phase separate into a GaN-rich solid solution phase at $x_{\text{Mn}} \sim 5\%$ and a secondary phase with no more than $x_{\text{Mn}}=50\%$.

C. Asymmetric x vs T phase diagram indicates high Curie temperature precipitates

Since we found that spinodal decomposition would lead to the formation of a Mn-rich alloy in the ZB phase with the approximate composition, $\text{Ga}_{0.5}\text{Mn}_{0.5}\text{N}$, or $x_{\text{Mn}}=50\%$, we now turn to predicting the magnetic properties of such a compound. Earlier predictions based on LDA calculations described alloys with $x_{\text{Mn}} > 25\%$ to have a nonferromagnetic spin-glass magnetic state.⁴³ However, since AF dominance is found to be reduced in the GGA+ U description for $x_{\text{Mn}}=100\%$, i.e., ZB MnN (Sec. IV), it is possible that alloys with $x_{\text{Mn}} > 25\%$ are in fact FM. We construct a 128 atom $\text{Ga}_{32}\text{Mn}_{32}\text{N}_{64}$ supercell consisting of four repeat units of a 32 atom SQS structure that models the random arrangement of Ga and Mn atoms. From the perspective of the mean-field approximation (MFA), the decisive quantity for the Curie temperature is $\Delta E_{\text{SD-FM}}$, i.e., the difference between the spin-disordered (SD) and the FM configurations. (Note that the failure of the MFA to account for percolation effects⁶² is not relevant for the high-concentration case considered here.) Thus, within the MFA, T_C is then determined by³⁹

$$T_C^{\text{MFA}} = \frac{1}{3k_B} \frac{S(S+1)}{S^2} \Delta E_{\text{SD-FM}}. \quad (5)$$

By sampling four different disordered spin configurations ($16 \times$ up and $16 \times$ down randomly distributed among the 32 Mn sites within the $\text{Ga}_{32}\text{Mn}_{32}\text{N}_{64}$ supercell), using GGA+ U , we determine $\Delta E_{\text{SD-FM}}=61(4)$ meV/Mn, which, using $S=2$ for the formal Mn (d^4) configuration, corresponds to a Curie temperature $T_C^{\text{MFA}}=354$ K just above room temperature. Thus, even though GGA+ U finds an FI state that is lowest in energy for pure MnN, the alloy with $x_{\text{Mn}}=50\%$ is clearly ferromagnetic, indicating that the composition dependent $T_C(x)$ is a nonmonotonic function.

VIII. DISCUSSION OF MAGNETISM IN ZINC-BLENDE (Ga,Mn)N ALLOYS WITH AND WITHOUT PHASE SEPARATION

Phase separation and precipitates have recently been invoked to explain the discrepancy between the calculated low

T_C of homogeneous ZB (Ga,Mn)N and the much higher measured values.^{43,62} Considering the homogeneous, random ZB-(Ga,Mn)N alloy, using LDA, one finds that the FM Mn-Mn interactions are strong only for the first nearest neighbors and decrease rapidly thereafter.^{43,47,63,64} The reason can be appreciated by considering the dilute limit where the Mn impurity forms a deep, midgap level in GaN with very localized wave functions so Mn-Mn wave functions overlap only at short Mn-Mn distances (unlike Mn in GaAs where the acceptor level is shallow and the wave function is extended).⁶⁵ Thus, quantitative Monte Carlo calculations based on the *ab initio* Mn-Mn exchange energies have shown that T_C of the homogeneous (Ga,Mn)N alloys are low (well below 100 K).^{62–64,66} [This is in contrast to earlier mean-field predictions proposing that (Ga,Mn)N can reach high T_C ferromagnetism, facilitated by the short Mn–N bond length and weak spin-orbit interaction⁴⁰.]

The discrepancy between the low T_C predicted for (Ga,Mn)N alloys via *ab initio* calculations of J_{ij} used in Monte Carlo simulation and the rather high T_C obtained via experiment prompted the suggestion of the role of precipitates and clusters (Ref. 43 and references therein). In general, clustering of an otherwise homogeneous alloy is expected to lower T_C because the cluster-cluster distances increase with increasing cluster size while the range of their magnetic interactions remain short ranged.^{63,64} However, spinodal phase separation can produce precipitates that contain far more Mn than the equivalent homogeneous alloy. Since ferromagnetism requires that the magnetic interactions percolate and since the percolation threshold for first nearest neighbors in the face-centered-cubic structure is $\sim 20\%$,⁴³ then precipitates can have $x_{\text{Mn}} > 20\%$ even if the homogeneous alloy has less. For (Ga,Mn)N, this scenario is problematic. Recall that LDA/GGA depicts Mn-rich zinc-blende (Ga,Mn)N alloys and MnN as having strong antiferromagnetic interactions [Fig. 1(a)], in contrast with ZB MnAs that is ferromagnetic. The effective increase in Mn concentration due to pure antiferromagnetic MnN precipitates would reduce T_C . GGA calculation of precipitates in low x_{Mn} (Ga,Mn)N alloys have shown a reduced T_C for increasing x_{Mn} , but an increased T_C

was found when the antiferromagnetic interactions were suppressed in the calculation using LDA+ U .⁴³

Our revised calculations show that the precipitates in (Ga,Mn)N may actually have a positive effect on T_C . The phase diagram [Fig. 8(b)] is asymmetric so precipitates have much less Mn than in the symmetric phase diagram obtained with simpler approximations. Thus, the eventual dominance of AF interactions in precipitates is reduced.

IX. CONCLUSIONS

MnN and (Ga,Mn)N alloys are investigated using the *ab initio* GGA+ U or the hybrid density-functional, B3LYP, formalisms. These methods are found to dramatically change electronic structure, magnetic moments, and relative stabilities compared to the more often used pure LDA or GGA methods. As a result, the experimentally observed rocksalt ground state of stoichiometric MnN is predicted in contrast to previous calculations where the fourfold zinc-blende structure is found to be most stable. The total energies of the various collinear magnetic configurations are investigated and suggest that the real configuration of zinc-blende MnN could be complex. Epitaxial calculations show that zinc-blende MnN can be stabilized on a InGaN substrate. (Ga,Mn)N alloys are investigated considering their structural stability, and a crossover at the Mn concentration of $x_{\text{Mn}} \sim 65\%$ from the zinc-blende-stable alloy to rocksalt-stable alloy was found. Cluster expansion calculations show the tendency for (Ga,Mn)N alloys to phase separate into precipitates consisting of Mn concentrations of ~ 5 and $\sim 50\%$. The latter is predicted to be ferromagnetic with $T_C = 354$ K in the mean-field approximation, indicating the possibility that ferromagnetism observed in (Ga,Mn)N alloys is due to the formation of Mn-rich precipitates in the zinc-blende phase.

ACKNOWLEDGMENTS

We thank S.-H. Wei for helpful comments. This work was funded by the U.S. Department of Energy, Office of Science, under NREL Contract No. DE-AC36-08GO28308.

¹K. Suzuki, T. Kaneko, H. Yoshida, Y. Obi, H. Fujimori, and H. Morita, *J. Alloys Compd.* **306**, 66 (2000).

²A. Leineweber, R. Niewa, H. Jacobs, and W. Kockelmann, *J. Mater. Chem.* **10**, 2827 (2000).

³M. S. Miao and W. R. L. Lambrecht, *Phys. Rev. B* **76**, 195209 (2007).

⁴M. S. Miao and W. R. L. Lambrecht, *Phys. Rev. B* **71**, 214405 (2005).

⁵H.-M. Hong, Y.-J. Kang, J. Kang, E.-C. Lee, Y.-H. Kim, and K. J. Chang, *Phys. Rev. B* **72**, 144408 (2005).

⁶H. Okuda, S. Senba, H. Sato, K. Shimada, H. Namatame, and M. Taniguchi, *J. Electron Spectrosc. Relat. Phenom.* **101-103**, 657 (1999).

⁷Y.-J. Zhao and A. Zunger, *Phys. Rev. B* **71**, 132403 (2005).

⁸K. Ono, J. Okabayashi, M. Mizuguchi, M. Oshima, A. Fujimori,

and H. Akinaga, *J. Appl. Phys.* **91**, 8088 (2002).

⁹T. W. Kim, H. C. Jeon, T. W. Kang, H. S. Lee, J. Y. Lee, and S. Jin, *Appl. Phys. Lett.* **88**, 021915 (2006).

¹⁰G. Prathiba, B. A. Naanci, and M. Rajagopalan, *J. Magn. Magn. Mater.* **309**, 251 (2007).

¹¹S. Sanvito and N. A. Hill, *Phys. Rev. B* **62**, 15553 (2000).

¹²W.-H. Xie, Y.-Q. Xu, B.-G. Liu, and D. G. Pettifor, *Phys. Rev. Lett.* **91**, 037204 (2003).

¹³A. L. Goodwin, M. G. Tucker, M. T. Dove, and D. A. Keen, *Phys. Rev. Lett.* **96**, 047209 (2006).

¹⁴R. Hines, N. Allan, G. Bell, and W. Mackrodt, *J. Phys.: Condens. Matter* **9**, 7105 (1997).

¹⁵J. M. Hastings, L. M. Corliss, W. Kunmann, and D. Mukamel, *Phys. Rev. B* **24**, 1388 (1981).

¹⁶S.-H. Wei and A. Zunger, *Phys. Rev. B* **48**, 6111 (1993).

- ¹⁷S.-H. Wei and A. Zunger, *Phys. Rev. Lett.* **56**, 2391 (1986).
- ¹⁸L. A. Kolodziejcki, R. L. Gunshor, N. Otsuka, B. P. Gu, Y. Hefetz, and A. V. Nurmikko, *Appl. Phys. Lett.* **48**, 1482 (1986).
- ¹⁹T. M. Giebultowicz, P. Klosowski, N. Samarth, H. Luo, J. K. Furdyna, and J. J. Rhyne, *Phys. Rev. B* **48**, 12817 (1993).
- ²⁰H. Akinaga, T. Manago, and M. Shirai, *Jpn. J. Appl. Phys., Part 2* **39**, L1118 (2000).
- ²¹J. H. Zhao, F. Matsukura, K. Takamura, E. Abe, D. Chiba, and H. Ohno, *Appl. Phys. Lett.* **79**, 2776 (2001).
- ²²J. F. Bi, M. G. Sreenivasan, K. L. Teo, and T. Liew, *J. Phys. D* **41**, 045002 (2008).
- ²³S. J. Pearton, C. R. Abernathy, G. T. Thaler, R. M. Frazier, D. P. Norton, F. Ren, Y. D. Park, J. M. Zavada, I. A. Buyanova, W. M. Chen, and A. F. Hebard, *J. Phys.: Condens. Matter* **16**, R209 (2004).
- ²⁴H. Ohno, *Science* **281**, 951 (1998).
- ²⁵B. Eck, R. Dronskowski, M. Takahashi, and S. Kikkawa, *J. Mater. Chem.* **9**, 1527 (1999).
- ²⁶B. R. Sahu and L. Kleinman, *Phys. Rev. B* **68**, 113101 (2003).
- ²⁷A. Janotti, S.-H. Wei, and L. Bellaiche, *Appl. Phys. Lett.* **82**, 766 (2003).
- ²⁸R. de Paiva, J. Alves, R. Nogueira, J. Leite, and L. Solfaro, *J. Magn. Magn. Mater.* **288**, 384 (2005).
- ²⁹W. R. L. Lambrecht, M. S. Miao, and P. Lukashev, *J. Appl. Phys.* **97**, 10D306 (2005).
- ³⁰P. Boguslawski and J. Bernholc, *Appl. Phys. Lett.* **88**, 092502 (2006).
- ³¹M. Marques, L. K. Teles, L. M. R. Solfaro, J. Furthmüller, F. Bechstedt, and L. G. Ferreira, *Appl. Phys. Lett.* **86**, 164105 (2005).
- ³²M. Marques, L. M. R. Solfaro, L. K. Teles, J. Furthmüller, F. Bechstedt, and L. G. Ferreira, *Appl. Phys. Lett.* **88**, 022507 (2006).
- ³³M. Ribeiro, Jr., M. Marques, L. M. R. Solfaro, L. K. Teles, and L. G. Ferreira, *Physics of Semiconductors: 28th International Conference of the Physics of Semiconductors*, AIP Conf. Proc. No. 893 (2007), p. 1227.
- ³⁴K. Suzuki, Y. Yamaguchi, T. Kaneko, H. Yoshida, Y. Obi, H. Fujimori, and H. Morita, *J. Phys. Soc. Jpn.* **70**, 1084 (2001).
- ³⁵H. Yang, H. Al-Britthen, E. Trifan, D. C. Ingram, and A. R. Smith, *J. Appl. Phys.* **91**, 1053 (2002).
- ³⁶S. Granville, B. J. Ruck, F. Budde, A. Koo, J. E. Downes, H. J. Trodahl, A. Bittar, N. Strickland, G. V. M. Williams, W. R. L. Lambrecht, T. Learmonth, K. E. Smith, V. J. Kennedy, A. Markwitz, and T. Schmitt, *Phys. Rev. B* **72**, 205127 (2005).
- ³⁷Although on-site Coulomb repulsion has been previously applied to Mn *d* levels in dilute (Ga,Mn)N alloys (Refs. 47 and 67), Mn clusters (Ref. 63), pure Mn selenides and tellurides (Ref. 68), and self-interaction correction on dilute (Ga,Mn)N (Ref. 69), no corrections of this sort have been applied to (Ga,Mn)N alloys with high Mn concentration or pure MnN. In addition, applying LDA+*U* (Refs. 47, 48, 67, and 70–74) and self-interaction corrections (Ref. 69) to (Ga,Mn)As has been shown to give good agreement with GGA-calculated electronic and magnetic structures, which agree well with experiment. Thus, MnN is unique among Mn and Cr pnictides and chalcogenides in that LDA/GGA fails to describe it.
- ³⁸G. M. Dalpian and S.-H. Wei, *J. Appl. Phys.* **98**, 083905 (2005).
- ³⁹J. C. Slater, *The Self-Consistent Field for Molecules and Solids*, Quantum Theory of Molecules and Solids Vol. 4 (McGraw-Hill, New York, 1974).
- ⁴⁰T. Dietl, H. Ohno, F. Matsukura, J. Cibert, and D. Ferrand, *Science* **287**, 1019 (2000).
- ⁴¹K. Sato and H. Katayama-Yoshida, *Jpn. J. Appl. Phys., Part 2* **46**, L1120 (2007).
- ⁴²K. Sato and H. Katayama-Yoshida, *Jpn. J. Appl. Phys., Part 2* **40**, L485 (2001).
- ⁴³H. Katayama-Yoshida, K. Sato, T. Fukushima, M. Toyoda, H. Kizaki, and P. H. Dederichs, *Phys. Status Solidi A* **204**, 15 (2007).
- ⁴⁴G. Kresse and J. Furthmüller, *VASP the Guide* (Universität Wien, Wien, Austria, 2007).
- ⁴⁵S. Lany, H. Raebiger, and A. Zunger, *Phys. Rev. B* **77**, 241201(R) (2008).
- ⁴⁶J. Okabayashi, A. Kimura, T. Mizokawa, A. Fujimori, T. Hayashi, and M. Tanaka, *Phys. Rev. B* **59**, R2486 (1999).
- ⁴⁷B. Sanyal, O. Bengone, and S. Mirbt, *Phys. Rev. B* **68**, 205210 (2003).
- ⁴⁸L. M. Sandratskii, P. Bruno, and J. Kudrnovský, *Phys. Rev. B* **69**, 195203 (2004).
- ⁴⁹A. D. Becke, *Phys. Rev. A* **38**, 3098 (1988); *J. Chem. Phys.* **98**, 5648 (1993); C. Lee, W. Yang, and R. G. Parr, *Phys. Rev. B* **37**, 785 (1988).
- ⁵⁰R. Dovesi, V. R. Saunders, C. Roetti, R. Orlando, C. M. Zicovich-Wilson, F. Pascale, B. Civalieri, K. Doll, N. M. Harrison, I. J. Bush, Ph. D'Arco, and M. Llunell, *CRYSTAL06 User's Manual* (University of Torino, Torino, 2007), <http://www.crystal.unito.it/>
- ⁵¹M. D. Towler, N. L. Allan, N. M. Harrison, V. R. Saunders, W. C. Mackrodt, and E. Apra, *Phys. Rev. B* **50**, 5041 (1994).
- ⁵²R. Pandey, J. Jaffe, and N. Harrison, *J. Phys. Chem. Solids* **55**, 1357 (1994).
- ⁵³J. Muscat, A. Wander, and N. M. Harrison, *Chem. Phys. Lett.* **342**, 397 (2001).
- ⁵⁴W. R. L. Lambrecht, M. Prikhodko, and M. S. Miao, *Phys. Rev. B* **68**, 174411 (2003).
- ⁵⁵J. E. E. Huber and D. Ridgley, *Phys. Rev.* **135**, A1033 (1964).
- ⁵⁶L. Chioncel, P. Mavropoulos, M. Ležaić, S. Blügel, E. Arrigoni, M. I. Katsnelson, and A. I. Lichtenstein, *Phys. Rev. Lett.* **96**, 197203 (2006).
- ⁵⁷B. Sanyal and O. Eriksson, *J. Appl. Phys.* **103**, 07D704 (2008).
- ⁵⁸B.-T. Liou, *Jpn. J. Appl. Phys.* **47**, 3350 (2008).
- ⁵⁹A. Zunger, S.-H. Wei, L. G. Ferreira, and J. E. Bernard, *Phys. Rev. Lett.* **65**, 353 (1990).
- ⁶⁰D. B. Laks, L. G. Ferreira, S. Froyen, and A. Zunger, *Phys. Rev. B* **46**, 12587 (1992).
- ⁶¹The cross-validation score is calculated as the average prediction error for a given number of ordered structures by the cluster expansion that is least-squares fitted from the rest of configurations in a data pool.
- ⁶²K. Sato, W. Schweika, P. H. Dederichs, and H. Katayama-Yoshida, *Phys. Rev. B* **70**, 201202(R) (2004).
- ⁶³T. Hynninen, H. Raebiger, and J. von Boehm, *Phys. Rev. B* **75**, 125208 (2007).
- ⁶⁴T. Hynninen, H. Raebiger, and J. von Boehm, *J. Phys.: Condens. Matter* **18**, 1561 (2006).
- ⁶⁵P. Mahadevan, J. M. Osorio-Guillén, and A. Zunger, *Appl. Phys. Lett.* **86**, 172504 (2005).
- ⁶⁶L. Bergqvist, O. Eriksson, J. Kudrnovský, V. Drchal, P. Korzhavyi, and I. Turek, *Phys. Rev. Lett.* **93**, 137202 (2004).

- ⁶⁷K. Sato, P. Dederichs, and H. Katayama-Yoshida, *Physica B* **376-377**, 639 (2006).
- ⁶⁸K. Nakamura, T. Akiyama, T. Ito, and A. J. Freeman, *J. Appl. Phys.* **103**, 07C901 (2008).
- ⁶⁹A. Filippetti, N. Spaldin, and S. Sanvito, *Chem. Phys.* **309**, 59 (2005).
- ⁷⁰A. B. Shick, J. Kudrnovský, and V. Drchal, *Phys. Rev. B* **69**, 125207 (2004).
- ⁷¹K. Sato, P. H. Dederichs, H. Katayama-Yoshida, and J. Kudrnovský, *J. Phys.: Condens. Matter* **16**, S5491 (2004).
- ⁷²J. Park, S. Kwon, and B. Min, *Physica B* **281-282**, 703 (2000).
- ⁷³K. Nakamura, K. Hatano, T. Akiyama, T. Ito, and A. J. Freeman, *Phys. Rev. B* **75**, 205205 (2007).
- ⁷⁴L. Bergqvist, B. Belhadji, S. Picozzi, and P. H. Dederichs, *Phys. Rev. B* **77**, 014418 (2008).